論文 / 著書情報
Article / Book Information

Title	Supramolecular liquid crystals from the dimer of L-shaped molecules with tertiary amide end groups
Authors	Yuki Sawatari, Yoshimichi Shimomura, Masato Takeuchi, Riki Iwai, Takuya Tanaka, Eiji Tsurumaki, Masatoshi Tokita, Junji Watanabe, Gen-ichi Konishi
Citation	Aggregate, Vol. 5, Issue 3, Page e507
Pub. date	2024, 1
DOI	https://doi.org/10.1002/agt2.507
Creative Commons	Information is in the article.

Received: 29 November 2023 | Revised: 21 December 2023 | Accepted: 6 January 2024

DOI: 10.1002/agt2.507

Aggregate WILEY

RESEARCH ARTICLE

Supramolecular liquid crystals from the dimer of L-shaped molecules with tertiary amide end groups

Yuki Sawatari[1] | **Yoshimichi Shimomura**[1] | **Masato Takeuchi**[2] | **Riki Iwai**[1] | **Takuya Tanaka**[1] | **Eiji Tsurumaki**[3] | **Masatoshi Tokita**[1,4] | **Junji Watanabe**[1,4] | **Gen-ichi Konishi**[1,4]

[1]Department of Chemical Science and Engineering, Tokyo Institute of Technology, Meguro-ku, Tokyo, Japan

[2]Department of Applied Chemistry, Osaka Metropolitan University, Sakai, Osaka, Japan

[3]Department of Chemistry, Tokyo Institute of Technology, Meguro-ku, Tokyo, Japan

[4]Department of Polymer Chemistry, Tokyo Institute of Technology, Meguro-ku, Tokyo, Japan

Correspondence
Gen-ichi Konishi, Department of Chemical Science and Engineering, Tokyo Institute of Technology, Ookayama, Meguro-ku, Tokyo 152-8552, Japan.
Email: konishi.g.aa@m.titech.ac.jp

Funding information
Japan Science and Technology Agency, Grant/Award Number: JPMJPR1096; Japan Society for the Promotion of Science, Grant/Award Numbers: 17H05145, 23H02036; Izumi Science and Technology Foundation

Abstract

Supramolecular liquid crystals (SLCs) are attractive materials for fabricating devices with new optoelectronic functions. Conventional SLCs are made from hydrogen-bonded mesogens. However, these mesogens suffer from high melting points, and the types of formable aggregates are limited owing to the directionality of the hydrogen bonding. Therefore, to fabricate non-hydrogen-bonded SLCs, we hypothesized that the introduction of tertiary amide groups into calamitic molecules would be advantageous because they have an L-shaped structure with *N*- or *C*-alkyl side chains not aligned along the long axis and the flexibility to undergo *cis–trans* isomerization. In this study, we developed a novel non-hydrogen-bonded SLC by assembling an L-shaped dimer composed of calamitic molecules (phenyltolanes) with tertiary amides at their ends. These molecules exhibited a smectic B phase. The phase transition temperature of the SLCs from crystal to liquid crystal phase was low despite the long π-conjugated core. Wide-angle X-ray diffraction and variable-temperature Fourier-transform infrared measurements revealed dimer formation by weak intermolecular interactions, that is, the molecular recognition of L-shaped molecules, and mobility of the alkyl groups attached to amide driven by *cis–trans* isomerization in the liquid crystal phase. Thus, *cis–trans* isomerization of tertiary amides contributed enormously to the formation and lower clearing points of this SLC. The developed method can be used not only to develop non-hydrogen-bonded SLCs but also to develop novel soft matter with controlled properties by incorporating the SLCs, as the aggregates can be controlled to impart desired functionalities.

KEYWORDS

mesogen, self-assembly, semectic phase, supramolecular liquid crystal, tertiary amide, variable-temperature Fourier-transform infrared

1 | INTRODUCTION

Supramolecular liquid crystals (SLCs)[1] are molecular assemblies that exhibit liquid crystallinity resulting from the complexation of small molecular components through non-covalent intermolecular interactions. SLCs usually comprise hydrogen-bonded mesogens, such as calamitic mesogens with a single hydrogen bond[2] and disk-shaped mesogens with multiple hydrogen bonds.[3] These hydrogen-bonded SLCs offer functionalities such as stimuli-responsiveness[4] and self-healing.[5] To further improve their functionality, it is important to design novel nano- or macro-scale molecules and self-assembled structures using SLCs. This requires controlling the aggregates constituting the liquid crystal phase, which is unique to SLCs, or forming new aggregates to improve the performance of functional materials.[6] This study focused on non-hydrogen-bonded SLCs, which have, thus far, not been extensively studied. Among the non-hydrogen-bonded SLCs reported so far are shuttle-type molecules[7] and dendrimers formed from cone-shaped dendrons.[8] Another example is metallomesogens,[9] which form through coordination bonds. Although coordination

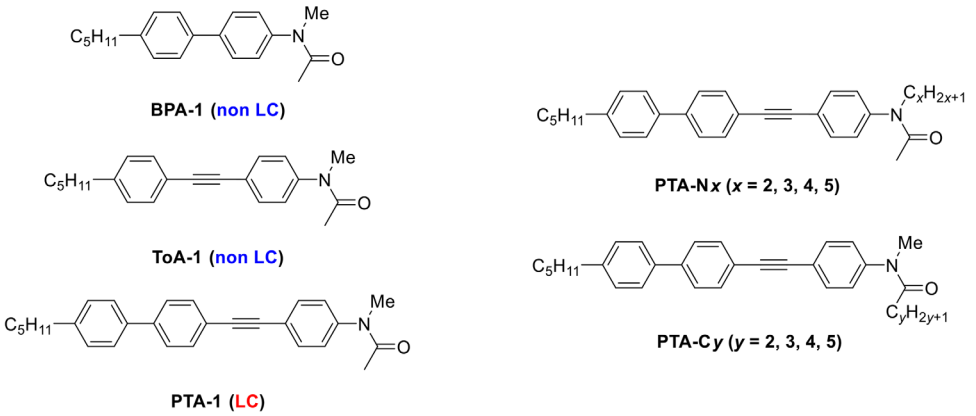

FIGURE 1 Chemical structures of BPA-1, ToA-1, PTA-1, PTA-N*x*, and PTA-C*y*.

bonds are classified as non-covalent, they are in fact equivalent to covalent bonds. Non-hydrogen-bonded SLCs can solve the problem of high melting points often exhibited by hydrogen-bonded SLCs and can be used to form various types of aggregates by utilizing non-directional interactions.[10] Entropy contributions owing to aggregate formation by weak intermolecular forces and shape recognition cannot be ignored. Thus, designing a non-hydrogen-bonded SLC is more difficult than designing a hydrogen-bonded SLC.

In this study, we focused on combining calamitic molecules and tertiary amides for the molecular design of novel non-hydrogen-bonded SLCs. While amide bonds have a more rigid structure than C—N single bonds because of the partial double-bond nature of the C—N bonds,[11] *N*-methylated tertiary amides are stable in the *cis*[12] but undergo *cis–trans* isomerization at low activation energies.[13] In addition, the *N*- or *C*-alkyl substituents of tertiary amides do not align in the long-axis direction of the molecules. We hypothesized that a dimeric mesogen is formed from L-shaped molecules with tertiary amides at the ends of the rigid core. Molecular assemblies that utilize the difference between *cis* and *trans* conformations are equally interesting. While SLCs formed from the hydrogen bonding of secondary amides have been previously reported,[14] SLCs comprising calamitic molecules with a tertiary amide have not yet been reported. Liquid crystals containing tertiary amides are rare, and a twist-bend nematic phase has been reported in which two molecules are linked by an alkylene group.[15] Here, we report a new class of SLCs that form non-hydrogen-bonded dimers by introducing tertiary amide and pentyl groups at the ends of phenyl tolanes. The SLCs exhibited much lower clearing points than hydrogen-bonded SLCs owing to *cis–trans* isomerization of the tertiary amides.

2 | RESULT AND DISCUSSION

2.1 | Molecular design

To find an appropriate rigid core for the non-hydrogen-bonded SLCs, we examined three types of compounds comprising π-conjugated moieties[16] with a pentyl group at one end and *N*-methylacetylamide at the other end: a biphenyl derivative of *N*-methyl-*N*-(4′-pentyl-[1,1′-biphenyl]-4-*yl*)acetamide (**BPA-1**), a tolane (diphenylacetylene) derivative of *N*-methyl-*N*-(4-((4-pentylphenyl)ethynyl)phenyl)acetamide (**ToA-1**), and a phenyl tolane derivative of *N*-methyl-*N*-(4′-((4-pentylphenyl)ethynyl)-[1,1′-biphenyl]-4-*yl*)acetamide (**PTA-1**) (Figure 1). Between these three compounds, only **PTA-1** with the longest π-conjugated skeleton exhibited liquid crystallinity as examined by polarized optical microscopy (POM) (Figures S2, S4, and S6) and differential scanning calorimetry (DSC) (Figures S1, S3, and S5). We developed two series of **PTA-1** homologs. One series is *N*-(4-((4′-pentyl-[1,1′-biphenyl]-4-*yl*)ethynyl)phenyl)-*N*-*x* alkylacetamide designated as **PTA-N*x*** (extended *N*-alkyl side) with x = 2–5. The other is *N*-methyl-*N*-(4′-((4-pentylphenyl)ethynyl)-[1,1′-biphenyl]-4-*yl*)-*C*-y alkylamide designated as **PTA-C*y*** (extended *C*-alkyl side) with y = 2–5 (Figure 1). To compare the phase transition temperatures of tertiary and secondary amide derivatives, the secondary amide **PTA-H-C4** (*N*-(4-((4′-pentyl-[1,1′-biphenyl]-4-*yl*)ethynyl)phenyl)pentanamide) was synthesized. All compounds were characterized by ^{1}H-NMR, ^{13}C-NMR, and high-resolution mass spectroscopy (HRMS). The detailed synthetic procedures are described in the Supporting Information (Section S1). The liquid crystallinities of the compounds were confirmed by DSC and POM, and wide-angle X-ray diffraction (WAXD) measurements were performed based on their phase transition temperatures.

2.2 | Phase transition behaviors

All compounds, except for **PTA-N2** (Figures S8 [DSC], S9 [POM], and S10 [WAXD]), exhibited liquid crystal phases. The phase transition behaviors of **PTA-group** (**PTA-1**, **PTA-N*x***, and **PTA-C*y***) (x, y = 2–5)) are summarized in Table 1. Thermogravimetric analysis (**TGA**) measurements were performed on **PTA-group** at a rate of 20°C min^{-1} (Figures S31–S39). **PTA-group** had no specific characteristics in phase transition. The phase transition temperatures were determined by DSC measurements (Figure 2B and Figures S5, S8, S11, S14, S17, S20, S23, and S26). **PTA-group** with longer alkyl chains had lower phase transition temperatures owing to the kinetic mobility of the alkyl chain. Furthermore, the elongation of the alkyl chains prevented crystallization (x or y = 4, 5) and resulted in a smectic E (SmE) phase with a thermodynamic stability similar to that of the SmB phase, showing polymorphism typical of liquid crystal molecules ($x \geq 4$, $y \geq 2$). In addition, comparing **PTA-N*x*** ($x \geq 3$)

TABLE 1 Phase transition temperature [°C] (enthalpy ΔH [kJ mol^{-1}]) of PTA-group upon heating (above line) and cooling (below line) at a rate of 10°C min^{-1}.

Entry	Cry	SmX	SmE	SmB'	SmB	N	Iso	d[b]	l[c]
BPA-1[a]	*56						*	–	
	–								
ToA-1	*81 (19.4)						*	–	
	*49 (−17.5)						*		
PTA-1	*178 (32.6)						*	26.8	23.3
	*150 (−13.2)				*166 (−12.8)	*169 (−0.9)	*		
PTA-N2	*167 (31.4)						*	–	23.3
	*145 (−29.9)						*		
PTA-N3	*134 (23.5)						*	29.5	23.6
	*116 (−8.8)				*126 (−13.3)		*		
PTA-N4			*102 (1.2)	*107 (0.4)	*115 (12.2)		*	30.5	24.2
			*100 (−1.3)		*112 (−12.1)		*		
PTA-N5			*88 (1.1)		*100 (11.7)		*	31.6	25.2
			*85 (−1.1)	*91 (−0.1)	*96 (−10.5)		*		
PTA-C2	*145 (9.73)		–		*150 (13.5)		*	28.5	24.7
	*126 (−6.8)		*132 (−1.8)		*147 (−13.5)		*		
PTA-C3	*121 (17.8)		–		*139 (13.9			29.5	26.2
	*63 (−9.2)		*118 (−1.6)		*136 (−13.6)		*		
						*			
PTA-C4			*105 (0.9)		*124 (8.1)		*	30.4	27.2
			*102 (−0.9)		*120 (−8.2)		*		
PTA-C5			*97 (1.2)		*120 (13.9)		*	31.6	28.6
			*94 (−1.2)		*117 (−13.8)		*		
PTA-H-C4[a]		237				*258	*	26.8	27.2
		237				*255	*		

[a]The phase transition temperature was determined by POM observation. Upon cooling, crystallization was not observed.
[b]Layer spacing of smectic phase calculated by WAXD measurement.
[c]Whole molecular length calculated using density functional theory (DFT) at the B3LYP/6-31G(d) level of theory.

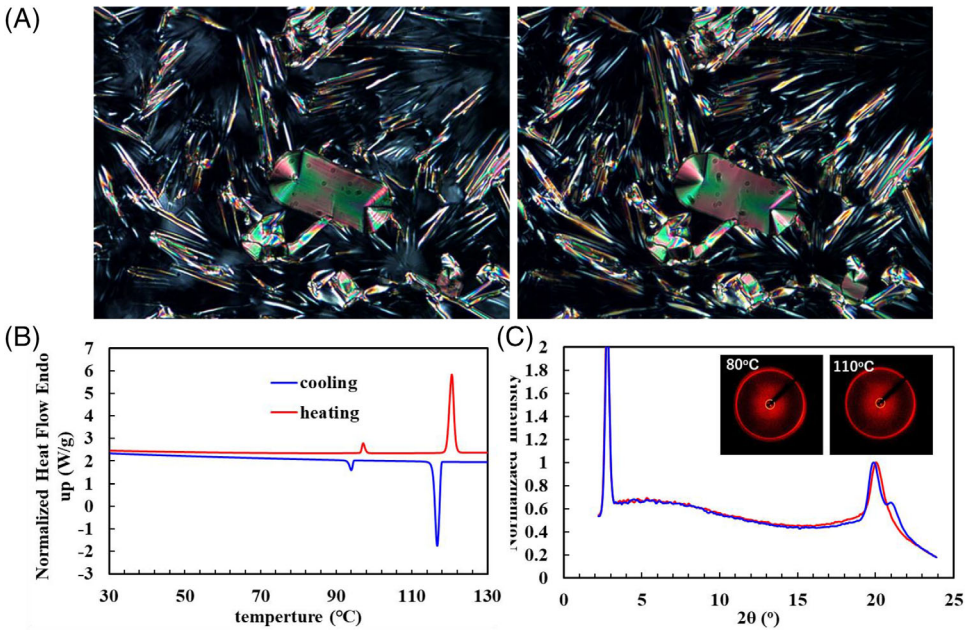

FIGURE 2 (A) POM images of PTA-C5 at 50°C (left) and 116°C (right) upon cooling. (B) DSC thermogram of PTA-C5 at a rate of 10°C min^{-1}. (C) WAXD intensity profiles of PTA-C5 at 80°C (blue line) and 110°C (red line) upon cooling.

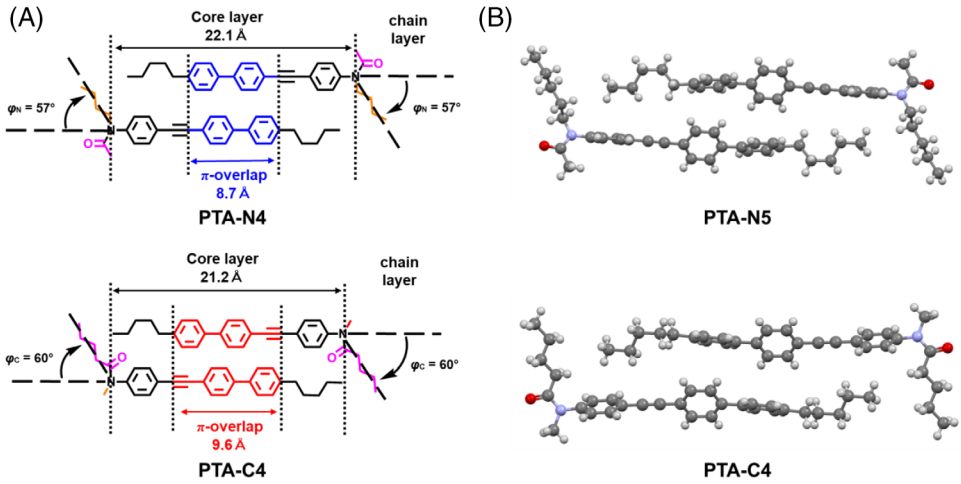

FIGURE 3 (A) Assumed molecular arrangements of PTA-N4 and PTA-C4 in the SmB phase. L-shaped molecules form an antiparallel dimer. (B) Dimer structures of PTA-N5 and PTA-C4, as observed by WAXD of the single crystal.

and **PTA-C*y*** ($y \geq 2$), the former tended to show less liquid crystallization.

PTA-1 and **PTA-N3** exhibited monotropic liquid crystal phases. Under POM, **PTA-1** displayed the schlieren texture characteristic of nematic liquid crystals for temperatures in the range of 166–169°C and the focal conic texture at 150–166°C (Figure S6). This focal conic texture is associated with a SmB phase. The WAXD pattern measured at 160°C (Figure S7) is characteristic of SmB phases, including two sharp peaks at diffraction angles (2θ) of 3.3 and 19.9° attributed to smectic layer spacing (d = 26.8 Å) and lateral distance (d = 4.5 Å) of mesogens arranged in short-range positional order. With further cooling, **PTA-1** crystallized at 150°C, displaying a concentric microstructure. **PTA-N3** formed an SmB phase, displaying lancet texture under POM (Figure S12). However, the WAXD patterns (Figure S13) included some reflections other than those characteristic of SmB phases, suggesting crystallization.

PTA-N*x* ($x \geq 4$) and all of the **PTA-C*y*** ($y \geq 2$) formed liquid crystal phases in both heating and cooling processes, including an SmB phase. These SmB phases, which were identified with lancet textures under POM (Figure 2A and Figures S15, S18, S21, S24, and S27) and WAXD (Figure 2C and Figures S16, S19, S22, S25, S28, and S30), transformed into different smectic phases, designated herein as SmB' or SmE, upon further cooling. The SmB phases transformed into another phase involving an enthalpy change (ΔH) < 0.5 kJ mol^{-1}, displaying a small endothermic peak in the heating DSC thermograms. However, as these phases appear similar to each other in the POM images and the WAXD patterns, we designate this phase as SmB'. **PTA-N*x*** ($x \geq 4$) and **PTA-C*y*** ($y \geq 2$) transformed the SmB phases into SmE phases, involving a change in ΔH of 0.9–1.8 kJ mol^{-1}. The changes in POM images and WAXD patterns are similar to those usually observed for the SmB–SmE transitions in other liquid crystal materials.[17] The SmE phases have the same layer spacing as the foregoing SmB phases, displaying WAXD patterns with a smectic layer reflection at the same 2θ as the foregoing SmB liquid crystals. In the wide-angle range ($2\theta \sim 20°$), the number of reflections increased from one to two, attributed to the evolution of the positional order of mesogens within a layer. Under a POM, the SmE phases showed concentric striations in the focal conic texture (Figure 2A and Figure S21).

As the clearing point of the secondary amide **PTA-H-C4** was above the upper temperature limit of the DSC instrument, the phase transition behavior was determined by POM observation. In the cooling process, **PTA-H-C4** exhibited a nematic phase in the 237–255°C range and a smectic phase (unidentified SmX phase shown in Table 1) at 25–237°C (Figure S29). **PTA-C4** had a clearing point 135°C lower than **PTA-H-C4**, despite having the same molecular structure.

2.3 | Molecular conformation and assembly in the SmB

PTA-N*x* (x = 3–5) and **PTA-C*y*** (y = 2–5) showed lancet textures observed in the SmB phase; however, the layer spacing value in the SmB phase was greater than the calculated length of the entire molecule (l) as the *trans* conformation (Table 1). This result suggests that in the smectic layers, cores are segregated from alkyl tails and overlap (Figure 3A).

We verified the validity of the assumed molecular arrangement in the SmB phase. For **PTA-N*x*** (x = 3–5) and **PTA-C*y*** (y = 2–5), the layer spacing measured for the SmB phases (d_{smectic}) was plotted against the number of carbon atoms on the backbone of the tertiary amide side tail counted from the carbon atom next to the N atom (Figure 3). Here, the number of atoms is equal to x and $y + 1$, respectively, for **PTA-N*x*** and **PTA-C*y***. The spacing is well fitted with a linear function of x (or $y + 1$). The spacing increases by Δd = 1.1 and 1.0 Å per x increase by 1 (or $y + 1$), respectively, for **PTA-N*x*** and **PTA-C*y***. When the alkyl tail extends perpendicularly from both sides of the core layer boundary, the increment of layer spacing is ~2 Å corresponding to twice the length of the methylene group.[18] Thus, the small value of Δd indicates that their alkyl tails are tilted against the layer.

The tilt angle from the smectic layer normal (φ_N, φ_C) was estimated to be $\varphi_N = 57°$ and $\varphi_C = 60°$, Equation (1a) for **PTA-N*x*** (x = 3–5) and Equation (1b) for **PTA-C*y*** (y = 2–5).

$$\varphi_N = \cos^{-1}\left(\frac{1.1}{2.0}\right) = 57^{\circ} \quad (1a)$$

$$\varphi_C = \cos^{-1}\left(\frac{1.0}{2.0}\right) = 60^{\circ} \quad (1b)$$

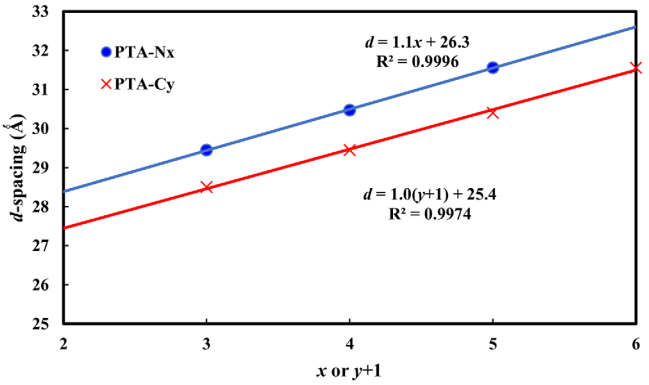

FIGURE 4 Layer spacing of the SmB phase against terminal chain length (x or $y + 1$).

The approximate lines in Figure 3 can be transformed into Equations (2a) and (2b).

$$d_{\text{smectic}}/\text{Å} = 2(0.55n + 2.1) + 22.1 \quad (2a)$$

$$d_{\text{smectic}}/\text{Å} = 2(0.50n + 2.1) + 22.2 \quad (2b)$$

The numbers 22.1 and 21.2 in Equations (2a) and (2b) indicate the thicknesses of the core layer because the other number represents the effective thickness of the alkyl chain-layer considering the van der Waals radius (=2.1 Å) of the terminal methyl. Considering the N atom of the amide as the terminal, the π-conjugated length of **PTA-group** was 15.4 Å (calculated using DFT at the B3LYP/6-31G(d) level of theory). Therefore, the overlapping rigid core (π-overlap) was 8.7 Å for **PTA-N*x*** and 9.6 Å for **PTA-C*y***. The resulting sequence of **PTA-group** in the smectic phase is shown in Figure 4A for an example of x and y values of 4.

Thus, the smectic layer spacing variation on the tail length suggests that **PTA-N*x*** and **PTA-C*x*** molecules bend at the tertiary amide group and are L-shaped. The formation of antiparallel dimers resulted in a stable structure because the electric dipole moments were offset. These dimeric structures were also observed in the single crystals of **PTA-N5** and **PTA-C4** (Figure 4B). All layers in the single crystal were composed of these dimer units (Figure S41). Therefore, dimers with L-shaped molecules are considered special, stable units. **PTA-N*x*** and **PTA-C*y*** ($x \geq 3$, $y \geq 2$) were SLCs because they appeared only in this dimer formation. As shown in Figure 4A, **PTA-C*y*** exhibited an ~0.9 Å-larger core layer and a wider liquid crystal temperature range than **PTA-N*x***. Therefore, controlling the core layer of the SLC of the **PTA-group** allows for adjustment of the liquid crystal temperature range.

2.4 | DFT calculations

The expansion of the amide alkyl chain in a single molecule was evaluated using DFT calculations (Figure 5).[19] Structural optimization of **PTA-N4** using DFT calculations at the B3LYP/6-31G(d) level yielded $\varphi_{N(\text{opt})} = 67°$, which is slightly larger than that estimated from the layer spacing $\varphi_{N(\text{WAXD})} = 57°$. The SmB phase was attributed to steric repulsion between the pentyl group at the biphenyl end and the alkyl chain of the tertiary amide during dimer formation.

For **PTA-C4** with the amide fixed in the *cis* or *trans* conformation, the structural optimization yielded $\varphi_{C(cis\ \text{opt})} = 78°$ and $\varphi_{C(trans\ \text{opt})} = 29°$, which are significantly larger and smaller, respectively, than that estimated from the layer spacings $\varphi_{C(\text{WAXD})} = 60°$, suggesting that the tertiary amide of **PTA-C4** in the liquid crystal state can assume the *cis* and *trans* conformations in equilibrium. Tertiary amides adopt either the most stable *cis* conformer or the metastable *trans* conformer,[20] crossing a rotational barrier at 14–16 kcal mol^{-1} (58–67 kJ mol^{-1}), which is low enough for isomerization at room temperature in an isolated system.[21] These results indicate that the tertiary amide was in equilibrium with both the *cis* and *trans* conformers present in the liquid crystal state.

The electrostatic potentials of **PTA-C5** and **PTA-N5** are shown in Figure S40. The antiparallel dimer structures were electrostatically stabilized because the carbonyl groups with the highest electron density were located far from each other. As shown in Figure S41, the electric interaction energies of the dimer structures (red colored pair) of **PTA-C4** and **PTA-N5** were −76.0 and −82.2 kJ mol^{-1}, respectively (using ωB97XD/6-311 g(d,p) level). ωB97XD was used here because it adds a long-range correction, which is not considered in B3LYP. ωB97XD was also used in the calculations because it has the advantage of low computational cost.[22] The electric interactions of dimers were sufficient. These calculation results correspond to the formation of antiparallel dimers within liquid crystal states. Note that in the liquid crystal state, the dimer interaction could not be calculated because of possible fluctuations due to molecular dynamics in addition to the *cis–trans* isomerization of the tertiary amide.

For further investigation, we performed variable-temperature Fourier-transform infrared (FT-IR) measurements in a diffuse reflectance mode.

2.5 | Variable-temperature FT-IR measurements

To discuss the relationship between the *cis–trans* isomerization of tertiary amides and the phase transition behavior, variable-temperature FT-IR measurements were performed. Figure 6A shows the diffuse reflectance spectra of a **PTA-C4** crystal sample under elevated temperatures in the range of 22.6–125°C. The typical absorption band attributed to the C═O stretching vibration of the amide group was observed at 1656 cm^{-1}. The absorption at 1656 cm^{-1} is attributed to the *cis* conformation of the amide group. When the temperature reached the clearing point of 125°C, a new absorption band appeared at higher wavenumber-regions of ~1680 cm^{-1}. The newly observed band at 1680 cm^{-1} suggests a change in the molecular conformation from *cis* to *trans* conformation. The spectral changes in FT-IR measurements exhibited a clear correspondence with the results of WAXD measurements, suggesting a transition from *cis* to *trans* conformation. Furthermore, at a measurement temperature exceeding the clearing point of 125°C, the absorption intensity of the IR spectrum significantly decreased because of a decrease in the sample area exposed to the IR beam as a result of the sample melting. When the sample was cooled from 125°C to room temperature (22.6°C), the absorption spectrum returned to its original shape, with the main absorption observed at

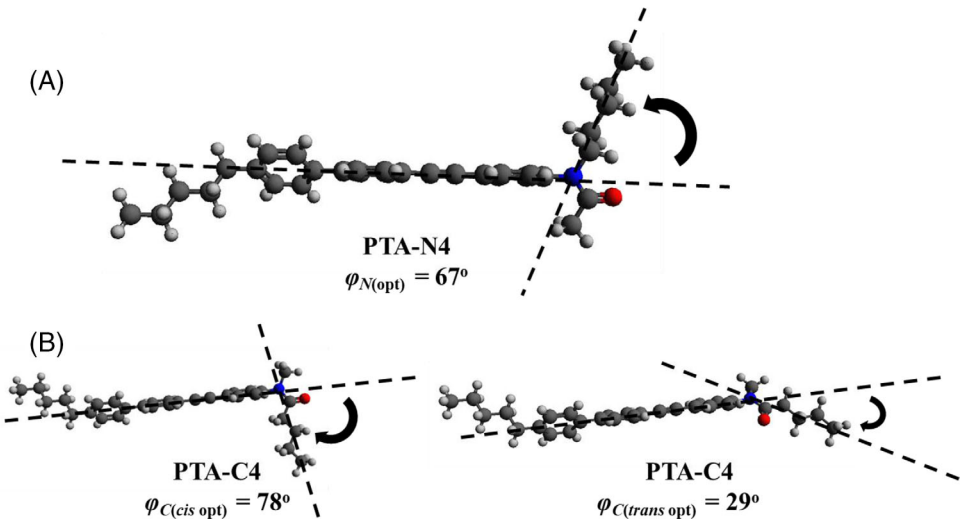

FIGURE 5 DFT optimized structures of PTA-N4 (A) and PTA-C4 (B) in *cis* conformation (left), and *trans* conformation (right), using B3LYP/6-311G level.

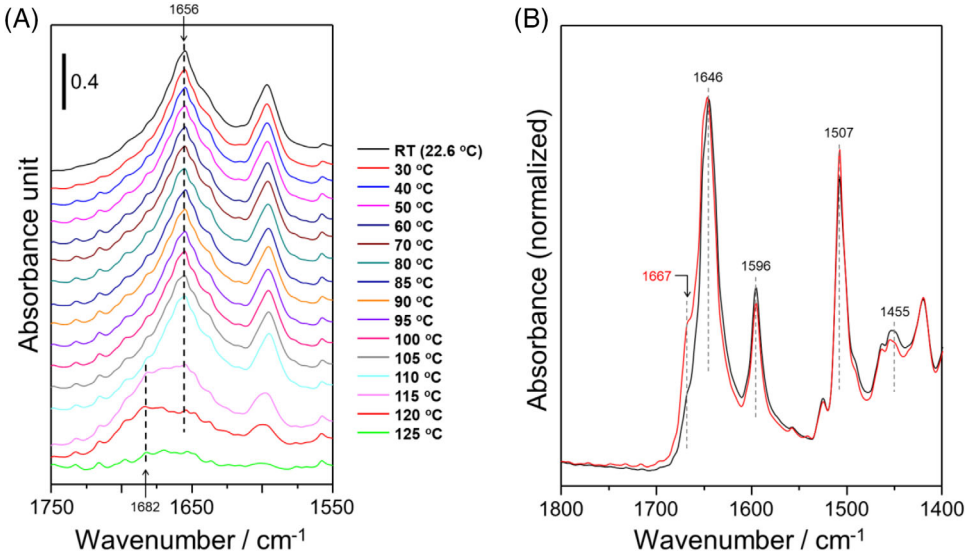

FIGURE 6 (A) Variable-temperature FT-IR spectra in a diffuse reflectance mode of PTA-C4 crystal sample under heating in the range of 22.6°C (room temperature) to 125°C. Absorption band derived from C═O in tertiary amide group is shown at 1656 cm^{-1} (*cis* form) and ~1682 cm^{-1} (*trans* form). (B) Room temperature ATR-FT-IR spectra of the PTA-C4 crystal sample (black) and the sample left at room temperature for several days after melting (red), normalized by the peak at 1646 cm^{-1}.

1656 cm^{-1}. However, the shoulder band at ~1680 cm^{-1}, attributed to the *trans* conformation of the amide, exhibited a slightly increased absorption intensity as compared with the sample before heating. This trend indicates that *cis*- and *trans*-conformations co-exist under 50°C, which is consistent with DSC results, in that **PTA-C4** is difficult to crystallize. Furthermore, similar results in the C═O stretching region of tertiary amide were obtained by attenuated total reflection (ATR) FT-IR measurements of the melted sample (Figure 6B), which had a higher resolution than the diffuse reflection method. Therefore, the results obtained by diffuse reflection are trustworthy.

2.6 | Optical properties

In the material science of liquid crystals, high birefringence is an important physical property. We measured the birefringence (Δn) of **PTA-1**, which exhibits a nematic phase, obtaining Δn = 0.29 at 550 nm, 169°C. In general, Δn = 0.1 or higher is required for application to birefringent materials,[23] making **PTA-1** suitable for this use.

Regarding application to organic materials, fluorescence properties are very important. The fluorescence wavelength (λ) and the quantum yield (Φ) of **PTA-C4** were measured (Figure S43), showing strong visible-light emission in the solid state (λ = 410 nm, Φ = 52%). Common organic molecules exhibit fluorescence quenching in aggregate states; hence, **PTA-C4** is seen to be suitable for solid-state fluorescent materials.

3 | SUMMARY

As illustrated in Figure 7, this study is summarized as follows: (1) In the crystal phase, the tertiary amide is fixed in

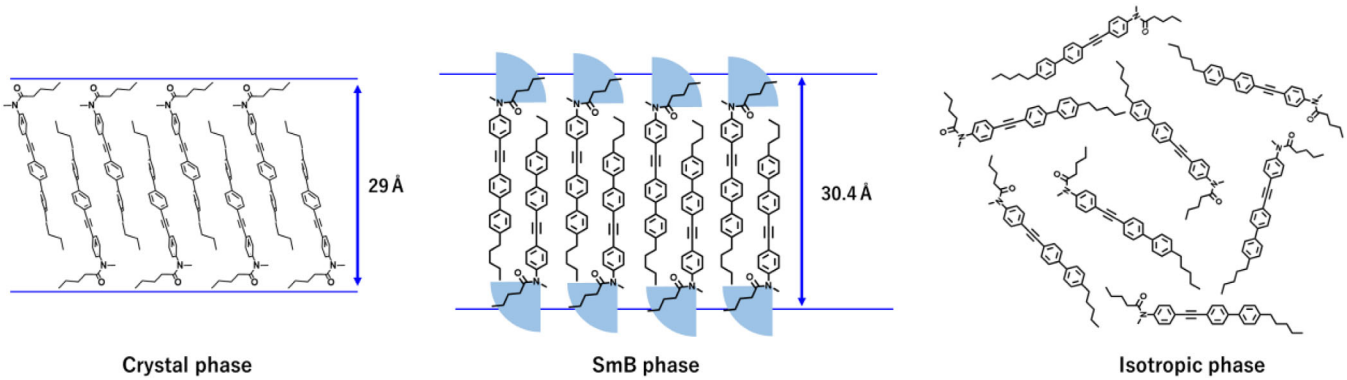

FIGURE 7 Conceptional diagram of molecular packing modes of PTA-C4 in crystal phase (left), SmB phase (center), and isotropic phase (right).

a stable *cis* conformation, and the L-shaped molecules form antiparallel dimers. The mesogens are tilted with respect to the normal layer due to intermolecular interactions. (2) In the SmB phase, the tertiary amides can undergo *cis–trans* isomerization despite forming L-shaped dimers. While dimers in the crystal phase are fixed in a pair, dimers in the liquid crystal phase can form pairs with molecules both above and below them, and an exchange is expected to occur continually. The liquid crystal phase is achieved by a balance between structural stabilization by interactions of π-conjugated systems and dynamics by *cis–trans* isomerization of the amide. The mesogens are aligned parallel to the layer normal, and the layer spacing is wider than in the crystal phase. The isotropization temperatures of non-hydrogen-bonded tertiary amide SLCs are lower than those of hydrogen-bonded secondary amide SLCs due to dimer formation by exchangeable mesogens and entropy increase by *cis–trans* isomerization of amides. (3) In the isotropic phase, the dimer structure is lost, and the molecules are free to move.

4 | CONCLUSION

We fabricated a non-hydrogen-bonded SLC by synthesizing a novel L-shaped molecule, **PTA-group**, which is a phenyl tolane derivative with a tertiary amide group at the end. **PTA-group** formed stable dimers despite the lack of hydrogen bonding. WAXD and variable-temperature FT-IR measurements revealed that both interactions of π-conjugated systems and the formation of L-shaped molecules and the *cis–trans* isomerization of tertiary amides contributed enormously to the formation of this SLC. In particular, **PTA-N*x*** (x = 4 and 5) and **PTA-C*y*** (y = 2–5) exhibited polymorphisms (some SmB and SmE phases), implying their potential to form various assemblies. Non-hydrogen-bonded SLCs have the advantages of low clearing points and the formability of direction-independent aggregates. The clearing point of **PTA-C4** was found to be 135°C lower than that of the secondary amide **PTA-H-C4**. In addition, as previously reported,[24] the clearing point of many hydrogen-bonded liquid crystals was above 150°C, even for mesogens that were shorter than the phenyl tolane. It has been suggested that the high melting point of hydrogen-bonded liquid crystals is due to the enormous aspect ratio of the mesogens because of aggregation.[25] By contrast, non-hydrogen-bonded liquid crystals are less effective at extending the aspect ratio owing to their weak interactions. Our newly developed method can expand the versatility of designing SLCs. Non-hydrogen-bonded supramolecules such as dendrons and shuttle-type molecules can be regarded as their smallest constituent units, as opposed to single molecules, which form the liquid crystal domain. By contrast, our tertiary amide **PTA-group** exhibits SLCs by forming small units without hydrogen bonds. Furthermore, this molecular design can be applied to various aggregates, liquid crystals,[26] organic crystals,[27] elastic crystals,[28] and polymeric aggregates.[29] Further functionalization of materials and developments of new soft materials can be expected by controlling the structures of aggregates or using mesogens of π-electron molecules with opt/electronic functions, such as introducing D-π-A structures.[30]

The introduction of **PTA-groups** into polymer side chains is expected to be applied to high-birefringence materials. While side-chain polymers using hydrogen-bonded SCLs have been reported,[31] side-chain polymers using non-hydrogen-bonded SCLs are yet to be studied. These polymers can be expected to have high anisotropy with low phase transition temperatures. Furthermore, **PTA-C4** is expected to be applied to solid-state fluorescent materials. In the future, we plan to study luminescence behavior in the liquid crystal phase to investigate its relationship with molecular packing.

ACKNOWLEDGMENTS

The authors thank Mr. Masato Koizumi (Materials Analysis Division, Tokyo Institute of Technology) for the HRMS measurements. The division is independent of our laboratory to ensure fairness. This project was supported in part by MEXT/JSPS KAKENHI grants 23H02036 and 17H05145 (Gen-ichi Konishi), JST Precursory Research for Embryonic Science and Technology (PRESTO) "Element Strategy" JPMJPR1096 (Gen-ichi Konishi), and the Izumi Science and Technology Foundation (Gen-ichi Konishi).

CONFLICT OF INTEREST STATEMENT

The authors declare no conflicts of interest.

DATA AVAILABILITY STATEMENT

The data that support the findings of this study can be obtained free of charge from The Cambridge Crystallographic Data Centre via www.ccdc.cam.ac.uk/data_request/cif (**PTA-N2**: CCDC2306937, **PTA-N5**: CCDC2308453, **PTA-C4**: CCDC2306936).

ORCID

Masato Takeuchi https://orcid.org/0000-0003-3851-9409
Gen-ichi Konishi https://orcid.org/0000-0002-6322-0364

REFERENCES

1. a) T. Kato, N. Mizoshita, K. Kishimoto, *Angew. Chem. Int. Ed.* **2005**, *45*, 38. b) C. M. Paleos, D. Tsiourvas, *Liq. Cryst*. **2001**, *28*, 1127. c) J. Uchida, B. Soberats, M. Gupta, T. Kato, *Adv. Mater.* **2022**, *34*, 2109063. d) S. J. D. Lugger, S. J. A. Houben, Y. Foelen, M. G. Debije, A. P. H. J. Schenning, D. J. Mulder, *Chem. Rev.* **2022**, *122*, 4946. e) H. Wang, H. K. Bisoyi, X. Zhang, F. Hassan, Q. Li, *Chem. Eur. J.* **2022**, *28*, e202103906. f) T. Kato, M. Gupta, D. Yamaguchi, K. P. Gan, M. Nakayama, *Bull. Chem. Soc. Jpn.* **2021**, *94*, 357. g) Y. Xu, A. Hao, P. Xing, *Angew. Chem. Int. Ed.* **2022**, *61*, e202113786. h) H. Wang, H. K. Bisoyi, B. Li, M. E. McConney, T. J. Bunning, Q. Li, *Angew. Chem. Int. Ed.* **2020**, *59*, 2684. i) Z.-L. Gong, Z.-Q. Li, Y.-W. Zhong, *Aggregate* **2022**, *3*, e177. j) R. J. Mandle, *Liq. Cryst.* **2022**, *49*, 2019.
2. a) T. Kato, J. M. J. Fréchet, *Macromolecules* **1989**, *22*, 3818. b) T. Kato, J. M. J. Fréchet, P. G. Wilson, T. Saito, T. Uryu, A. Fujishima, C. Jin, F. Kaneuchi, *Chem. Mater.* **1993**, *5*, 1094. c) T. Kato, J. M. J. Fréchet, *J. Am. Chem. Soc.* **1989**, *111*, 8533. d) U. Kumar, T. Kato, J. M. J. Fréchet, *J. Am. Chem. Soc.* **1992**, *114*, 6630. e) T. Kato, P. G. Willson, A. Fujishima, J. M. J. Fréchet, *Bull. Chem. Soc. Jpn.* **1990**. *12*, 2003. f) Y. Arakawa, Y. Sasaki, H. Tsuji, *J. Mol. Liq.* **2019**, *280*, 153.
3. a) A. Kraft, A. Reichert, R. Kleppinger, *Chem. Commun.* **2000**, *12*, 1015. b) R. Kleppinger, C. P. Lillya, C. Yang, *Angew. Chem. Int. Ed.* **1995**, *34*, 1637. c) M. Suárez, J.-M. Lehn, S. C. Zimmerman, A. Skoulios, B. Heinrich, *J. Am. Chem. Soc.* **1998**, *120*, 9526.
4. a) K. Kanie, M. Nishii, T. Yasuda, T. Taki, S. Ujiie, T. Kato, *J. Mater. Chem.* **2001**, *11*, 2875. b) K. Kanie, T. Yasuda, S. Ujiie, T. Kato, *Chem. Commun.* **2000**, *19*, 1899. c) H. Zhang, X. Chang, C. Ma, G. Huang, B. S. Li, B. Z. Tang, *ACS Appl. Mater. Interfaces* **2022**, *14*, 43926. d) F. Song, Y. Cheng, Q. Liu, Z. Qiu, J. W. Y. Lam, L. Lin, F. Yang, B. Z. Tang, *Mater. Chem. Front.* **2019**, *3*, 1768. e) W. Zhang, S. Suzuki, T. Sakurai, H. Yoshida, Y. Tsutsui, M. Ozaki, S. Seki, *Phys. Chem. Chem. Phys.* **2020**, *22*, 28393.
5. a) N. L. Slack, M. Schellhorn, T. Eiselt, M. A. Chibbaro, U. Schulze, H. E. Warriner, P. Davidson, H.-W. Schmidt, C. R. Safinya, *Macromolecules* **1998**, *31*, 8503. b) H. E. Warriner, S. H. J. Idziak, N. L. Slack, P. Davidson, C. R. Safinya, *Science* **1996**, *271*, 969. c) S. J. D. Lugger, S. J. A. Houben, Y. Foelen, M. G. Debije, A. P. H. J. Schenning, D. J. Mulder, *Chem. Rev.* **2022**, *122*, 4946.
6. a) T. Kato, N. Mizoshita, *Curr. Opin. Solid State Mater. Sci.* **2002**, *6*, 579. b) T. Kato, *Science* **2002**, *295*, 2414. c) J. van Haaren, D. J. Broer, *Chem. Ind.* **1998**, *24*, 1017. d) S. I. Stupp, V. LeBonheur, K. Walker, L. S. Li, K. E. Huggins, M. Keser, A. Amstutz, *Science* **1997**, *276*, 384.
7. a) M. Sawamura, K. Kawai, Y. Matsuo, K. Kanie, T. Kato, R. Nakamura, *Nature* **2002**, *419*, 702. b) Y. Matsuo, A. Muramatsu, R. Hamasaki, N. Mizoshita, T. Kato, E. Nakamura, *J. Am. Chem. Soc.* **2004**, *126*, 432.
8. a) V. Percec, W.-D. Cho, G. Ungar, *J. Am. Chem. Soc.* **2000**, *122*, 10273. b) V. Percec, W.-D. Cho, P. E. Mosier, G. Ungar, D. J. P. Yeardley, *J. Am. Chem. Soc.* **1998**, *120*, 11061. c) G. Ungar, Y. Liu, X. Zeng, V. Percec, W.-D. Cho, *Science* **2003**, *299*, 1208.
9. a) R. Giménez, D.P. Lydon, J.L. Serrano, *Curr. Opin. Solid State Mater. Sci.* **2002**, *6*, 527. b) A.-M. Giroud-Godquin, P. M. Maitlis, *Angew. Chem. Int. Ed.* **1991**, *30*, 375. c) F. Vera, J. L. Serranoa, T. Sierra, *Chem. Soc. Rev.* **2009**, *38*, 781.
10. The twist bend nematic phase is another type of supramolecular liquid crystal. It is formed by dimers of two mesogens connected by a linker. a) P. A. Henderson, C. T. Imrie, *Liq. Cryst.* **2011**, *38*, 1407. b) M. Cestari, S. Diez-Berart, D. A. Dunmur, A. Ferrarini, M. R. de la Fuente, D. J. B. Jackson, D. O. Lopez, G. R. Luckhurst, M. A. Perez-Jubindo, R. M. Richardson, J. Salud, B. A. Timimi, H. Zimmermann, *Phys. Rev. E* **2011**, *84*, 031704. c) R. J. Mandle, *Molecules* **2022**, *27*, 2689. d) Y. Arakawa, K. Komatsu, H. Tsuji, *New J. Chem.* **2019**, *43*, 6786. e) D. A. Paterson, R. Walker, J. M. D. Storey, C. T. Imrie, *Liq. Cryst.* **2023**, *50*, 725.
11. J. Bandekar, *Biochim. Biophys. Acta, Protein Struct. Mol. Enzymol.* **1992**, *1120*, 123.
12. Kagan recommends stereoisomers of secondary and tertiary amides should be described in *E/Z* notation. H. B. Kagan, *Organic Stereochemistry*, Hodder Arnold, London **1977**. However, conventionally, the conformation in which the molecule stretches in the rod-shaped direction is described as *trans*. In the study of the physical properties od amides, the *cis/trans* notation, which does not follow the nomenclature, is easier to understand.
13. I. Azumaya, T. Okamoto, F. Imabeppu, H. Takayanagi, *Tetrahedron* **2003**, *59*, 2325.
14. a) Y. Kobayashi, Y. Matsunaga, *Bull. Chem. Soc. Jpn.* **1987**, *60*, 3515. b) Y. Harada, Y. Matsunaga, N. Miyajima, S. Sakamoto, *J. Mater. Chem.* **1995**, *5*, 2305. c) Y. Matsunaga, N. Miyajima, Y. Nakayasu, S. Sakai, M. Yonenaga, *Bull. Chem. Soc. Jpn.* **1988**, *61*, 207.
15. a) G. J. Strachan, W. T. A. Harrison, J. M. D. Storey, C. T. Imrie, *Phys. Chem. Chem. Phys.* **2021**, *23*, 12600. b) G. J. Strachan, A. Zattarin, J. M. D. Storey, C. T. Imrie, *J. Mol. Liq.* **2023**, *384*, 122160.
16. a) Y. Arakawa, S. Kang, H. Tsuji, J. Watanabe, G. Konishi, *RSC Adv*. **2016**, *6*, 92845. b) Y. Arakawa, S. Kang, H. Tsuji, J. Watanabe, G. Konishi, *RSC Adv*. **2016**, *6*, 16568. c) Y. Arakawa, S. Kang, S. Nakajima, Y. Cho, S. Kawauchi, J. Watanabe, G. Konishi, *J. Mater. Chem. C* **2013**, *1*, 8094. d) Y. Arakawa, S. Nakajima, R. Ishige, M. Uchimura, S. Kang, G. Konishi, J. Watanabe, *J. Mater. Chem.* **2012**, *22*, 8394.
17. a) P. A. C. Gane, A. J. Leadbetter, J. J. Benattar, F. Moussa, M. Lambert, *Phys. Rev.* **1981**, *24*, 2694. b) Z.-Q. Yu, T.-T. Li, Z. Zhang, J.-H. Liu, W. Z. Yuan, J. W. Y. Lam, S. Yang, E.-Q. Chen, B. Z. Tang, *Macromolecules* **2015**, *48*, 2886.
18. a) S. Krimm, *J. Polym. Sci. Polym. Lett. Ed.* **1980**, *18*, 687. b) C. Tanford, *J. Phys. Chem.* **1974**, *78*, 2469.
19. M. J. Frisch, G. W. Trucks, H. B. Schlegel, G. E. Scuseria, M. A. Robb, J. R. Cheeseman, G. Scalmani, V. Barone, G. A. Petersson, H. Nakatsuji, X. Li, M. Caricato, A. V. Marenich, J. Bloino, B. G. Janesko, R. Gomperts, B. Mennucci, H. P. Hratchian, J. V. Ortiz, A. F. Izmaylov, J. L. Sonnenberg, D. Williams-Young, F. Ding, F. Lipparini, F. Egidi, J. Goings, B. Peng, A. Petrone, T. Henderson, D. Ranasinghe, et al., *Gaussian 16, Revision C.01*, Gaussian, Inc., Wallingford, CT **2016**.
20. a) S. Saito, Y. Toriumi, N. Tomioka, A. Itai, *J. Org. Chem.* **1995**, *60*, 4715. b) Y. K. Kang, *J. Mol. Struct.* **2001**, *546*, 183.
21. a) M. Ōki, *Topics in Stereochemistry* (Eds: N.L. Allinger, E.L. Eliel, S.H. Wilen), Vol. *14*, Wiley, Hoboken, NJ **1983**. b) X. Guan, S. Wang, G. Shi, J. Zhang, X. Wan, *Macromolecules* **2021**, *54*, 4592.
22. S. Tsuzuki, T. Uchimaru, *Phys. Chem. Chem. Phys.* **2020**, *22*, 22508.
23. a) X. Chen, B. Zhang, F. Zhang, Y. Wang, M. Zhang, Z. Yang, K. R. Poeppelmeier, S. Pan, *J. Am. Chem. Soc.* **2018**, *140*, 16311. b) M. Yamaguchi, M. E. A. Manaf, K. Songsurang, S. Nobukawa, *Cellulose* **2012**, *19*, 601.
24. a) D. J. Prince, H. Adams, D. W. Bruce, *Mol. Cryst. Liq. Cryst.* **1996**, *289*, 127. b) T. Kato, J. M. J. Frechet, P. G. Wilison, T. Saito, T. Uryu, A. Fujishima, C. Jin, F. Kaneuchi, *Chem. Mater*, **1993**, *5*, 1094.
25. Y. Arakawa, S. Kang, J. Watanabe, G. Konishi, *RSC Adv*. **2015**, *5*, 8056.
26. a) J. Yuan, X. Lu, Q. Lu, *Aggregate*, **2023**, e431, DOI: 10.1002/agt2.431. b) P. Zhou, K. Han, *Aggregate* **2022**, *3*, e160. c) Y. He, S. Lin, J. Guo, Q. Li, *Aggregate* **2021**, *2*, e141. d) J. Voskuhl, M. Giese, *Aggregate* **2022**, *3*, e124. e) V. Percec, D. Sahoo, *Giant* **2022**, *12*, 100127. f) Z. Zheng, H. Hu, Z. Zhang, B. Liu, M. Li, D.-H. Qu, H. Tian, W.-H. Zhu, B. L. Feringa, *Nat. Photon*. **2022**, *16*, 226. g) S. Cho, H. Yoshida, M. Ozaki, *Adv. Opt. Mater.* **2020**, *8*, 2000375. h) M. Uchimura, Y. Watanabe, F. Araoka, J. Watanabe, H. Takezoe, G. Konishi, *Adv. Mater.* **2010**, *22*, 4473.
27. a) M. Gao, J. Ren, Y. Gong, M. Fang, J. Yang, Z. Li, *Aggregate*, **2023**, e462, DOI: 10.1002/agt2.462. b) H. Rao, Z. Liu, M. Chen, C. Zheng, L. Xu, J. Liu, J. W. Y. Lam, B. Li, X. Yang, B. Z. Tang, *Aggregate*, **2023**, e453, DOI: 10.1002/agt2.453. c) Y. Liu, X. Yang, L. Ye, H. Ma, H. Zhu, *Aggregate* **2023**, *4*, e347. d) J. Deng, Z. Zhang, P. Sang, S. Yin, S. Zhang, Y. Li, B. Yang, C. Gu, Y. Ma, *Aggregate* **2023**, *4*, e313. e) M. Shimizu, T. Sakurai. *Aggregate* **2022**, *3*, e144. f) K. Wada, K. Hashimoto, J. Ochi, K. Tanaka, Y. Chujo, *Aggregate* **2021**, *2*, e93. g) J. Yang, M. Fang, Z. Li, *Aggregate* **2020**, *1*, 6. h) K. Takagi, D. Miyamoto, H. Yamaguchi, I. Azumaya, *Bull. Chem. Soc. Jpn.* **2022**, *95*, 47. i) Y. Shimomura, K. Igawa, S. Sasaki, N. Sakakibara, R. Goseki, G. Konishi, *Chem. Eur. J.* **2022**, *28*, e202201884. j) S. Suzuki, S. Sasaki, A. S. Sairi, R. Iwai, B. Z. Tang, G. Konishi, *Angew. Chem. Int. Ed.* **2020**, *59*, 9856. k) R. Iwai, S. Suzuki, S. Sasaki, A. S. Sairi, K. Igawa, T. Suenobu, K. Morokuma, G. Konishi, *Angew. Chem. Int. Ed.* **2020**, *59*, 10556. l) S. Sasaki, S. Suzuki, W. M. C. Sameera, K. Igawa, K. Morokuma, G. Konishi, *J. Am. Chem. Soc.* **2016**, *138*, 8194. m) J. Ochi, K. Yuhara, K. Tanaka, Y. Chujo, *Chem. Eur. J.* **2022**, *28*, e202200155. n) A. Huang, Y. Fan, K. Wang, Z. Wang, X. Wang, K. Chang, Y. Gao, M. Chen, Q. Li, Z. Li, *Adv. Mater.* **2023**, *35*, 2209166. o) A. N. Sussardi, G. F. Turner, J. G. Richardson, M. A. Spackman, A. T. Turley, P. R. McGonigal, A. C. Jones, S. A. Moggach, *J. Am. Chem. Soc.* **2023**, *145*, 19780.

28. a) T. Matsuo, K. Ikeda, S. Hayashi, *Aggregate* **2023**, *4*, e378. b) S. Hayashi, T. Koizumi, *Angew Chem. Int. Ed.* **2016**, *55*, 2701. c) S. Hayashi, *Bull. Chem. Soc. Jpn.* **2022**, *95*, 721.
29. a) J. Yuan, X. Lu, Q. Lu, *Aggregate*, **2023**, e431, DOI: 10.1002/agt2.431. b) Y. He, S. Lin, J. Guo, Q. Li, *Aggregate* **2021**, *2*, e141. c) G. Zhang, X. Cheng, Y. Wang, W. Zhang, *Aggregate* **2022**, *4*, 262. d) Y. Shimomura, M. Tokita, A. Kawamura, J. Watanabe, G. Konishi, *Macromolecules* **2023**, *56*, 5152. e) H. Yan, Y. He, D. Wang, T. Han, B. Z. Tang, *Aggregate* **2023**, *4*, e331. f) H. Ikebe, K. Nakao, E. Hisamura, M. Furukori, Y. Nakayama, T. Hosokai, M. Yang, G. Liu, T. Yasuda, K. Albrecht, *Aggregate*, **2023**, e405, DOI: 10.1002/agt2.405. g) S. Segawa, X. Ou, T. Shen, T. Ryu, Y. Ishii, H. H. Y. Sung, I. D. Williams, R. T. K. Kwok, K. Onda, K. Miyata, X. He, X. Liu, B. Z. Tang, *Aggregate*, **2023**, e499, DOI: 10.1002/agt2.499. h) J. Kida, D. Aoki, H. Otsuka, *Aggregate* **2021**, *2*, e50.
30. a) Y. C. Hu, S. Y. Yin, W. Liu, Z. H. Li, Y. Chen, J. S. Li, *Aggregate* **2023**, *4*, e256. b) B. Kumari, R. Dahiwadkar, S. Kanvah, *Aggregate* **2022**, *3*, e191. c) H. Shen, Y. Li, Y. Li, *Aggregate* **2020**, *1*, 57. d) Y. Shimomura, G. Konishi, *Chem. Eur. J.* **2023**, *29*, e202301191. e) Y. Niko, S. Kawauchi, G. Konishi, *Chem. Eur. J.* **2013**, *19*, 9760. f) S. Sasaki, G. P. C. Drummen, G. Konishi, *J. Mater. Chem. C* **2016**, *4*, 2731. g) H. Wang, Q. Li, P. Alam, H. Bai, V. Bhalla, M. R. Bryce, M. Cao, C. Chen, S. Chen, X. Chen, Y. Chen, Z. Chen, D. Dang, D. Ding, S. Ding, Y. Duo, M. Gao, W. He, X. He, X. Hong, Y. Hong, J.-J. Hu, R. Hu, X. Huang, T. D. James, X. Jiang, G.-i. Konishi, R. T. K. Kwok, J. W. Y. Lam, C. Li, et al. *ACS Nano* **2023**, *17*, 14347. h) C. Micheletti, Q. Wang, F. Ventura, M. Turelli, I. Ciofini, C. Adamo, A. Pucci, *Aggregate* **2022**, *3*, e188.
31. T. Kato, H. Kihara, U. Kumar, T. Uryu, J. M. J. Fréchet, *Angew. Chem. Int. Ed.* **1994**, *33*, 1644.

SUPPORTING INFORMATION

Additional supporting information can be found online in the Supporting Information section at the end of this article.

How to cite this article: Y. Sawatari, Y. Shimomura, M. Takeuchi, R. Iwai, T. Tanaka, E. Tsurumaki, M. Tokita, J. Watanabe, G. Konishi, *Aggregate* **2024**, e507. https://doi.org/10.1002/agt2.507